Formic acid dehydrogenation attained by Pd nanoparticles-based catalysts supported on MWCNT-C_3N_4 composites

Miriam Navlani-García, David Salinas-Torres, Francisco Daniel Vázquez-Álvarez, Diego Cazorla-Amorós

PII: S0920-5861(21)00327-8

DOI: https://doi.org/10.1016/j.cattod.2021.07.019

Reference: CATTOD13445

To appear in: *Catalysis Today*

Received date: 29 March 2021
Revised date: 28 June 2021
Accepted date: 14 July 2021

Please cite this article as: Miriam Navlani-García, David Salinas-Torres, Francisco Daniel Vázquez-Álvarez and Diego Cazorla-Amorós, Formic acid dehydrogenation attained by Pd nanoparticles-based catalysts supported on MWCNT-C_3N_4 composites, *Catalysis Today,* (2021) doi:https://doi.org/10.1016/j.cattod.2021.07.019

Formic acid dehydrogenation attained by Pd nanoparticles-based catalysts supported on MWCNT-C_3N_4 composites

Miriam Navlani-García[1*], David Salinas-Torres[2], Francisco Daniel Vázquez-Álvarez[1], Diego Cazorla-Amorós[1]

[1]*Departamento de Química Inorgánica e Instituto de Materiales, Universidad de Alicante, Apartado 99, Alicante, E-03080, España*

[2]*Departamento de Química Física e Instituto de Materiales, Universidad de Alicante, Apartado 99, Alicante, E-03080, España*

***Corresponding Author*:** miriam.navlani@ua.es. Miriam Navlani-García, Departamento de Química Inorgánica e Instituto Universitario de Materiales, University of Alicante, P.O. Box 99, San Vicente del Raspeig, E-03080, Alicante, Spain. Phone number: +34965903946.

Abstract

In this study, we developed Pd nanoparticles-based catalysts supported on composites formed by multi-walled carbon nanotubes (MWCNTs) and graphitic carbon nitride (*g*-C_3N_4) in various proportions, for their use in the dehydrogenation of formic acid in the liquid phase. It was observed that the composition of the support determined the average size of the Pd nanoparticles as well as their electronic properties, which ultimately affected the performance of Pd/MWCNT-C_3N_4 catalysts. Among assessed, the catalyst with 63 wt.% of C_3N_4 exhibited the best activity, with an initial TOF value of 4258 h^{-1} calculated based on the surface Pd atoms.

Keywords:

Hydrogen production, formic acid, Pd nanoparticles, carbon nitride, multi-walled carbon nanotubes, composite support.

1.Introduction

The ever-increasing demand for energy together with fossil fuel depletion and the environmental issues derived from their use is fostering the search for alternative energy sources. Among the alternatives to fossil fuels, the use of hydrogen (H_2) is undoubtedly one of the most interesting solutions towards the development of a carbon-free-based energy system. Although H_2 does not exist naturally on Earth, it can be produced from both non-renewable energy sources (i.e. coal, oil, and natural gas) and renewable energy sources, such as solar, wind, and biomass energy, thus overcoming the limitation of other energy sources which are subjected to fluctuations and temporal and geographical unequal distributions.

Hydrogen has a gravimetric energy content of 143 MJ kg^{-1}, which is three times larger than liquid hydrocarbon-based fuels. However, its very low density in the gaseous state (0.08988 g/L at 1 atm), and the high energy consumption of the liquefaction process required for its storage, are major drawbacks for its use as a fuel [1]. Then, finding alternative ways to store hydrogen is crucial to fully deploy the so-called hydrogen economy. Among the options investigated, chemical hydrogen storage offers very interesting possibilities. Numerous hydrogen carrier molecules are being fruitfully explored, both in the solid and liquid phase [2]. In this context, the production

of H_2 from liquid organic hydrogen carriers (LOHC) has received a tremendous promise, since they enable safe and efficient high-density hydrogen storage in an easy-to-handle way, hence eliminating the need for pressurized tanks for storage and transportation [3,4].

LOHCs exist as liquids or low melting point solids under ambient storage conditions. They have a pair of hydrogen-lean and hydrogen-rich molecules [5]. Hydrogen is stored *via* catalytic hydrogenation of the hydrogen-lean molecules and released by catalytic dehydrogenation reaction of the hydrogen-rich counterpart [6,7].

Several LOHCs have been explored [3,8–11] and, even though their application in the energy storage scenario is not as mature as other technologies, research works addressing the utilization of LOHCs started nearly four decades ago [6,11,12]. Among them, formic acid, the simplest carboxylic acid (HCOOH, FA) has drawn great attention in the last decade [13–23]. Its properties as an auspicious hydrogen carrier molecule have been highlighted in the recent literature [24–29]. FA has a relatively high content of hydrogen (4.4 wt. %), and it is a stable liquid at room pressure and temperature, it has low toxicity and flammability and can be achieved by the hydrogenation of CO_2 [30,31]. Its application within the sustainable energy scenario is backed up by the fact that FA can be produced from several biomass-derived feedstocks through hydrolysis, wet oxidation, and catalytic oxidation reactions [32,33].

Catalytic dehydrogenation of FA to produce H_2 has been attained by both homogeneous and heterogeneous catalysts and most of the recent efforts are being devoted to those heterogeneous catalysts constituted by metal nanoparticles (NPs) stabilized onto supports of diverse nature with functional groups surface modifications. Among them, Pd-based catalysts have given very interesting results [17,18,22,25,27,34]. Nitrogen-doped carbon materials are one the preferred supports

since they attain excellent results derived from the stabilization of the metal active phase and the modification of the electronic properties of the metal NPs [2,35–37]. Also, nitrogen functional groups may actively participate in the dehydrogenation reaction by interacting with the molecules of FA thus increasing the local concentration of the reactant in the vicinity of the catalytic active sites [36,37]. The N-containing carbon supports used are prepared from in-situ doping methods or post-synthetic strategies [2], which frequently require several reaction steps or harsh experimental conditions. With this in mind, exploring the utilization of other N and C-rich-containing molecules is a promising alternative to those N-doped carbon materials.

In this work, we developed Pd based catalysts supported on composites formed by multi-walled carbon nanotubes (MWCNTs) and graphitic carbon nitride (*g*-C_3N_4). The performance of Pd/MWCNT-C_3N_4 catalysts with various compositions of the support was assessed in the dehydrogenation of FA in the liquid phase. It was observed that the catalysts supported on MWCNT-C_3N_4 displayed very small and well-distributed Pd NPs, which was attributed to the abundant anchoring sites offered by the nitrogen groups of C_3N_4 that is wrapping the surface of the MWCNTs. The electronic properties of the Pd NPs also depended on the composition of the support. It was seen that, among investigated, Pd/MWCNT-C_3N_4(63) was the most promising catalyst, affording an initial TOF of 4258 h^{-1} calculated based on the surface Pd atoms.

2. Experimental

2.1 Synthesis of g-C_3N_4

For the synthesis of *g*-C_3N_4, 5 g of dicyandiamide were placed in a covered alumina crucible and were heated up to 520 ºC for 4 h (with a heating rate of 5 ºC/min) under an air atmosphere [38,39].

2.2. Synthesis of MWCNT-C_3N_4 supports

Multiwalled carbon nanotubes (from Nanoblack Columbian Chemicals Co (GA, USA)) were used for the preparation of MWCNTs-C_3N_4 supports. For that, a fixed amount of MWCNT (0.75 g) was dispersed in 20 mL of water by using an ultrasonic bath for 30 min. After that, an aqueous solution of the C_3N_4 precursor (i.e. dicyandiamide) was added to the MWCNTs dispersion, and the resulting mixture was heated at 100 ºC and was kept under stirring until complete solvent removal. Various concentrations of dicyandiamide were used to achieve supports with different compositions. Once the water was evaporated, the resulting solid was grinded smoothly to ensure a homogeneous blending. The resulting material was heat-treated at 520 ºC for 4 h (heating rate of 5 ºC/min) under a nitrogen atmosphere to obtain C_3N_4 from its precursor. After that, the composite supports were grinded and collected. They were denoted as MWCNT-C_3N_4(x), being "x" the C_3N_4 wt. % determined from the nitrogen content obtained by elemental analysis (*vide infra*).

2.3. Synthesis of Pd/MWCNT-C_3N_4 catalysts

Pd-based catalysts were prepared by the standard impregnation method with Na_2PdCl_4 and subsequent reduction with $NaBH_4$. 0.75 g of the MWCNT-C_3N_4(x) support were dispersed in 150 mL of water and the adequate amount of a solution of Na_2PdCl_4 was added to achieve a final Pd loading of 1 wt.%. The mixture was stirred for 1 h at room temperature and, after that, a fresh solution of $NaBH_4$ (with a Pd/$NaBH_4$ molar ratio of 1/5) was added dropwise while stirring the solution. Then, it was stirred for 1 h more, and it was filtered, washed and dried overnight. Pd/MWCNT and Pd/C_3N_4 were prepared with the same experimental procedure.

2.4. Characterization of the materials

The nitrogen content was determined by elemental analysis using a microanalyzer Thermo Finnigan Flash 1112. X-ray diffraction (XRD) patterns were registered in the 2θ range of 10-80° using a Miniflex II Rigaku with Cu K_α radiation. Nitrogen adsorption-desorption isotherms were carried out at -196 °C using an automatic adsorption system (Micromeritics ASAP 2020 analyzer). The samples were outgassed at 250 °C for 4 h to remove any possible adsorbed impurity. The apparent surface area (S_{BET}) and total micropore volume (V_{DR} N_2) were calculated applying the Brunauer-Emmett-Teller (BET) method and the Dubinin-Radushkevich (DR) equation, respectively. The total pore volume was calculated at a relative pressure of $P/P_0 = 0.95$ [40]. Pd loading was determined by Inductively Coupled Plasma-Optical Emission Spectroscopy (ICP-OES) with a Perkin-Elmer Optima 4300 system. The morphology of the samples was observed by Transmission Electron Microscopy (TEM). The average NP size was determined from representative micrographs registered by TEM after measuring ~ 100 particles with the ImageJ software.

X-ray photoelectron spectroscopy (XPS) analysis was conducted in a VG-Microtech Multilab 3000 spectrometer equipped with a semispherical electron analyzer and a Mg Kα (hv=1253.6 eV) 300 W X-ray source. The analysis chamber has a flood gun to avoid the charging effect. All the binding energies were referred to the C 1s line at 284.6 eV. C 1s, N 1s, and Pd 3d were analyzed. The different species of C, N and Pd were assigned from the deconvoluted spectra. A Shirley line was used to estimate the background signal.

2.5. Catalytic tests

The activity of the Pd/MWCNT-C_3N_4(x) catalysts in the dehydrogenation of formic acid was evaluated by following the gas evolution during 30 minutes of reaction at 75 ºC. The tests were carried out with 0.15 g of catalyst and the reaction mixture, which consisted of an aqueous solution of formic acid and sodium formate with a molar ratio of 9 to 1 (final concentration of 1 M). The catalyst is placed in the reactor once 75 ºC have been reached, so the temperature is fixed along the reaction course. The gas evolution was followed using a burette system. The set-up consists of a reactor (of 50 mL), immersed in an oil bath to keep the reaction temperature (i.e. 75 ºC), which is connected to a cooling system and a graduated tube filled with water. Constant stirring of (~ 700 rpm) is kept by using a magnetic stirrer in the reactor. The starting time of the reaction is set when the solution of formic acid is incorporated into the reactor. Pd/MWCNT and Pd/C_3N_4 were also assessed as reference catalysts. TOF values (h^{-1}) were calculated with the following equation:

$$\text{TOF } (h^{-1}) = \frac{\text{Produced } H_2 \text{ (mole)}}{\text{Pd atoms (mole)} \times \text{time (h)}}$$

The produced H_2 (mole) is the mole of H_2 generated after 1 min of reaction, and Pd atoms are determined from the Pd content obtained by ICP-OES analysis. TOF values were also calculated considering only the surface Pd atoms, which were calculated from the TEM average NP size (d_{TEM}) and Pd NP dispersion (D_{TEM}) [37].

3. Results

The supports were characterized by elemental analysis to know their real composition. The nitrogen content (wt. %) determined and the content of C_3N_4 calculated from those results are included in Table 1.

Table 1. Composition of the supports determined by elemental analysis.

Support	wt. % N	wt. % C_3N_4
MWCNTs	-	-
MWCNT-C_3N_4(16)	10.3	16.3
MWCNT-C_3N_4(38)	23.7	37.6
MWCNT-C_3N_4(46)	28.8	45.7
MWCNT-C_3N_4(63)	39.8	63.1
g-C_3N_4	63.0	-

The structure of the MWCNT-C_3N_4 composites was checked by XRD. Figure 1 contains the diffractograms of raw MWCNT and C_3N_4, together with the patterns achieved for the composite materials. The XRD pattern for the MWCNT contains the (002) and (100) peaks at 2θ = 25.6 and 42 degrees, respectively, related to the graphite-like structure. The diffractogram of *g*-C_3N_4 has two diffraction peaks located at 2θ = 27.5, ascribed to the reflection from the (002) planes corresponding to the typical interlayer stacking of this material, and 2θ = 13.0, ascribed to the planes in planar tris-s-triazine structural packing motifs [38,39]. Interestingly, the XRD profiles for MWCNT-C_3N_4(x) composites are very similar to that of pure MWCNT, even for the material with the highest *g*-C_3N_4 content. The results suggest that either very small and disperse domains of C_3N_4 are formed onto the surface of MWCNTs or that a low crystallinity (or amorphous) C_3N_4 phase grows mediated by the MWCNT.

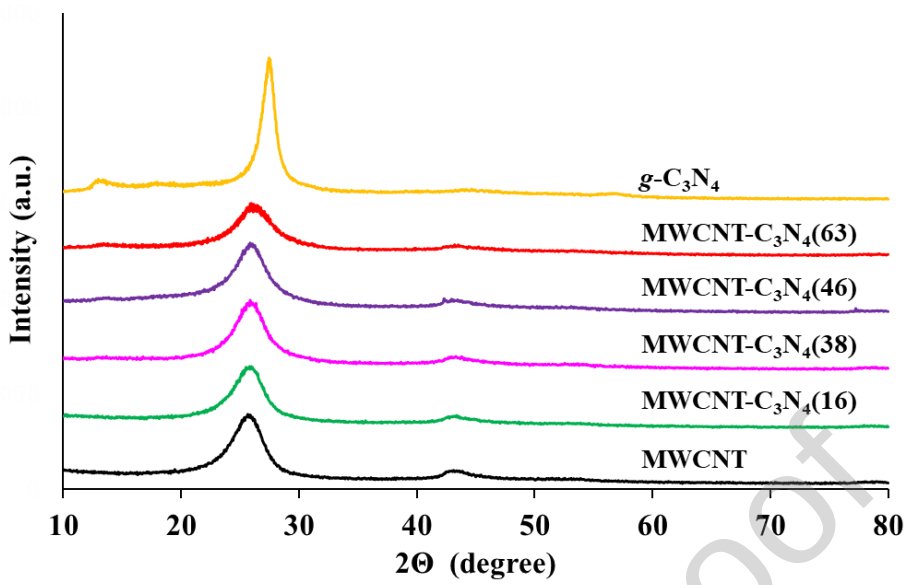

Figure 1. XRD patterns of MWCNTs, *g*-C_3N_4, and MWCNT-C_3N_4 composites.

Figure 2 shows the N_2 adsorption-desorption isotherms of both pristine materials (MWCNT and g-C_3N_4) and their composites. Table 2 summarizes the most important porous texture data. The N_2 isotherms for both pristine materials are typical of non-porous solids in which the hysteresis observed is due to capillary condensation that occurs in the voids between particles [40]. The BET surface area obtained for the MWCNT is in agreement with typical values for carbon nanotubes [41]. The low surface area for the pristine *g*-C_3N_4 is also in agreement with the values found for this material in the literature and is a consequence of the strong layer stacking. Interestingly, the porosity data determined for the composite materials do not follow the mixtures law and are much lower than expected. For example, the composite with a *g*-C_3N_4 content of only 16 wt. % presents an apparent surface area of 160 m^2 g^{-1}, which is a reduction of S_{BET} value by almost half of the S_{BET} of MWCNTs. These results can be explained considering that *g*-C_3N_4 growth on the surface of the MWCNT (this is observed in TEM images, see Figure S1) can favor particle aggregation due to the strong layer-layer interaction in *g*-C_3N_4.

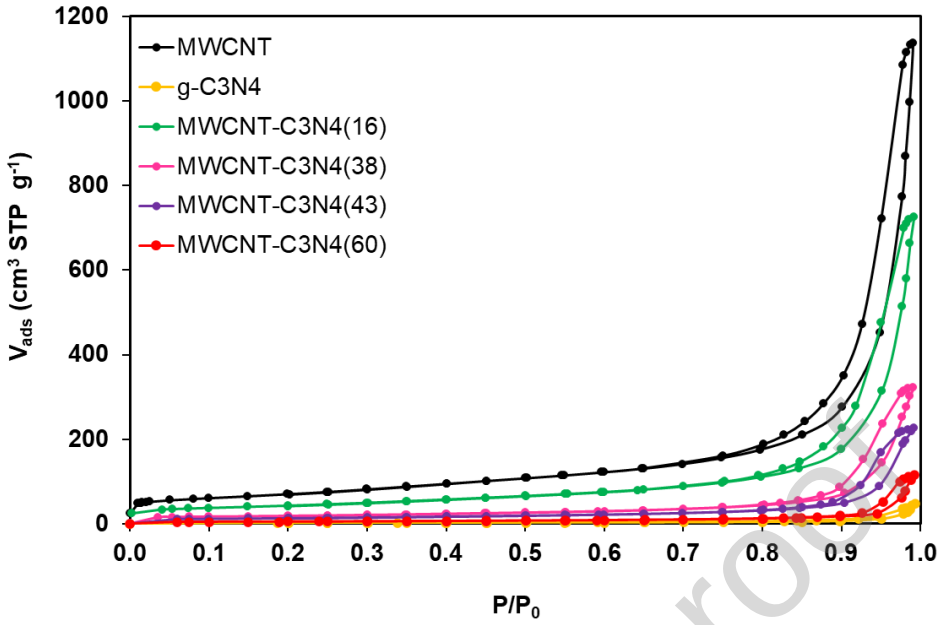

Figure 2. N_2 adsorption-desorption isotherms at -196 ºC for MWCNT, g-C_3N_4, and their MWCNT-C_3N_4 composites.

Table 2. Pore texture for the pristine supports and their composites.

Sample	S_{BET} / $m^2 g^{-1}$	$V_{DR}N_2$ / $cm^3 g^{-1}$	V_t^* / $cm^3 g^{-1}$
MWCNTs	260	0.10	0.70
g-C_3N_4	6	-	0.02
MWCNT-C_3N_4(16)	160	0.06	0.49
MWCNT-C_3N_4(38)	70	0.03	0.22
MWCNT-C_3N_4(46)	45	0.02	0.14
MWCNT-C_3N_4(63)	20	0.01	0.04

* Total pore volume (P/P_0 = 0.95)

Table 3 contains information about the characterization of the different studied catalysts. ICP results indicated that Pd was successfully loaded onto the supports and the actual metal content was very close to the nominal Pd loading (1 wt. %). The slightly lower metal loading achieved might be due to the washing and drying steps performed during the preparation of the samples. Table 3 also contains information about the surface Pd content (at. %) determined by XPS.

The morphology of the catalysts can be seen in Figure 3, which contains representative micrographs of all samples together with the pertinent histograms with the NP size distributions. The calculated average NP size and dispersion are listed in Table 3. From Pd/MWCNT-C_3N_4 catalysts, it can be seen that the MWCNTs are wrapped with the C_3N_4, thus ensuring intimate contact between both components of the composites.

It was observed that, despite the different average NPs size measured for catalysts with different compositions, all of them exhibited spherical and well-distributed NPs and significant aggregation of the NPs was not detected, even for those catalysts with lower external surface area, such as Pd/C_3N_4. That observation may be due to the important stabilizing effect of *g*-C_3N_4, which contains abundant nitrogen groups serving as the anchoring sites for the metal NPs [38,42,43]. The average NPs size determined in the catalysts strongly depended on the composition of the supports. The average NP size measured for the catalysts with pure MWCNTs and *g*-C_3N_4 was determined to be 4 ± 4, and 6 ± 2 nm, respectively, while smaller NPs were achieved for Pd/MWCNT-C_3N_4(x) catalysts, which exhibited very small Pd NPs, with an average NP size of ~ 2 nm. Such small and well-distributed NP achieved in the catalysts with MWCNT-C_3N_4(x) may be due to the presence of homogeneous domains of C_3N_4 on the surface of the MWCNTs, so that the nitrogen functional groups serve as more efficient anchoring points for the metal NPs than those nitrogen groups present on the pristine C_3N_4. In the case of pristine C_3N_4, its low surface area and efficient layer stacking make that a large amount of those N ligand sites are not available. This, in turns, suggests that the high external surface area of MWCNT and its 1D structure, plays a key role in offering a suitable platform for the distribution of C_3N_4, thus creating abundant and available anchoring sites for the stabilization of the NPs.

Table 3. Pd content (wt. %), surface Pd content (at. %), and average NP size (nm) determined in the catalysts.

Catalyst	Pd loading (wt. %, ICP)	Surface Pd (at. %, XPS)	Average NP size (nm)	D_{TEM} (%)
Pd/MWCNTs	0.82	0.19	4. ± 4	22.5
Pd/MWCNT-C_3N_4(16)	0.70	0.24	1.6 ± 0.5	56.3
Pd/MWCNT-C_3N_4(38)	0.69	0.47	2.2 ± 0.4	40.9
Pd/MWCNT-C_3N_4(46)	0.75	1.34	2.3 ± 0.6	39.1
Pd/MWCNT-C_3N_4(63)	0.78	2.03	2.4 ± 0.8	37.5
Pd/C_3N_4	0.71	3.41	6 ± 2	15.0

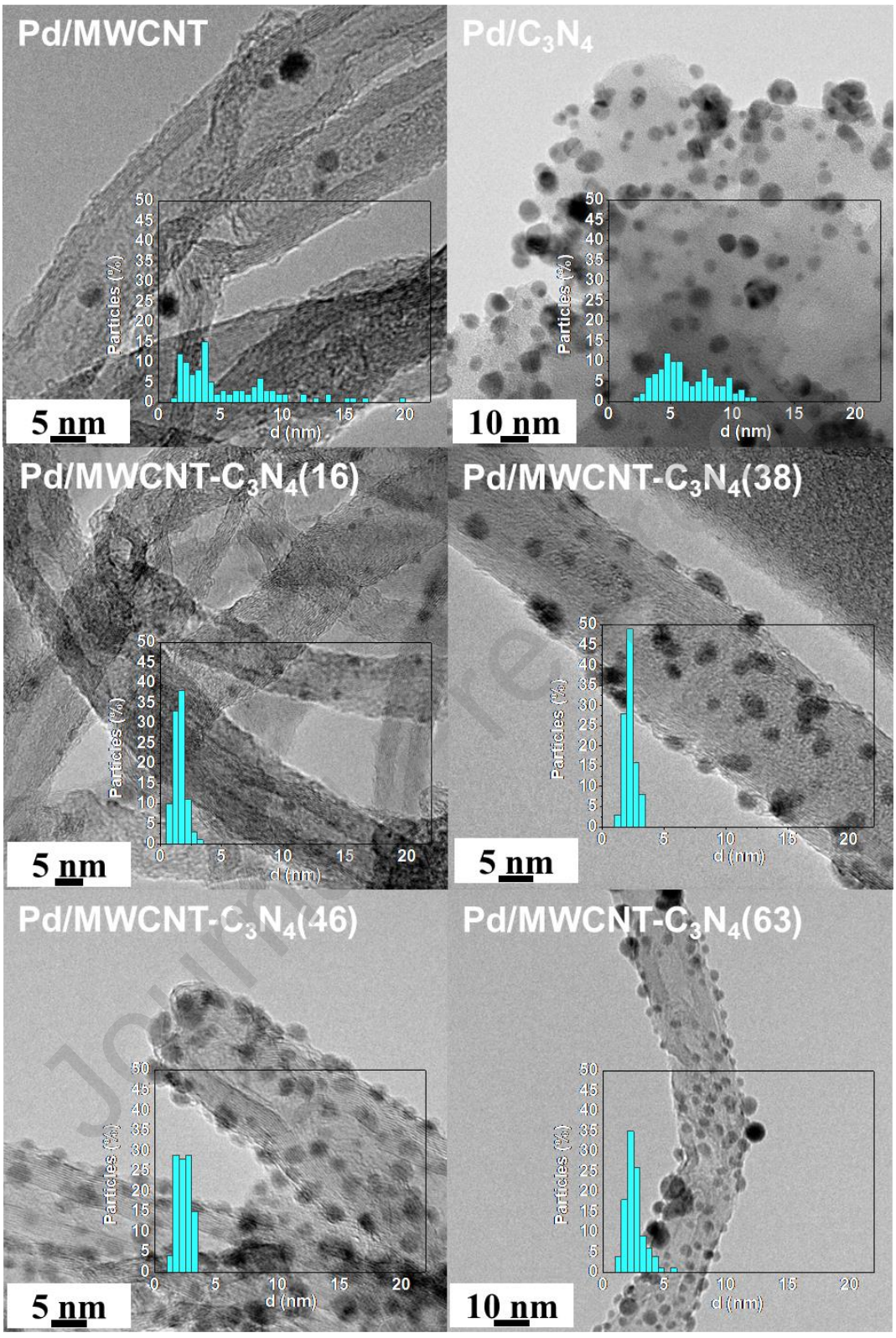

Figure 3. TEM micrographs of Pd/MWCNT, Pd/C_3N_4, and Pd/MWCNT-C_3N_4(x) catalysts, and their corresponding histogram with the NP size distribution.

XPS analysis was performed to get information about the electronic properties of the different species (See Figure 4). N 1s XPS spectrum in *g*-C_3N_4 is characterized by three peaks that appeared at 398.4 eV for the nitrogen atoms in the triazine and heptazine rings (-C=N-C), 399.9 eV for tertiary nitrogen (N-$(C)_3$), which are the central nitrogen atoms that link the triazine and heptazine units, and 400.8 eV for positively charged N species or quaternary N species [44,45]. Pd/MWCNT-C_3N_4(16)-(46) showed the same XPS spectra as Pd/C_3N_4, confirming the formation of C_3N_4 in the pertinent composite supports. However, the N spectrum of the catalyst with the largest proportion of C_3N_4 (Pd/MWCNT-C_3N_4(63)) is different. It displayed the peaks associated with the nitrogen atoms in the triazine and heptazine rings, the tertiary nitrogen (N-$(C)_3$) and the positively charged nitrogen species; however, a new peak located at 397.1 eV appears. Such low binding energy peak has been attributed to the presence of N species bonded to sp^3 carbon in amorphous CN structures. It has been postulated that the lower binding energy of such species is due to the lone pair of electrons that screen the N 1s electrons, thus further reducing the N 1s energy [46]. This lone pair of electrons are not delocalized in the CN framework due to the N atom being bonded to sp^3 C atoms. This is in good agreement with the C 1s XPS spectra of Pd/MWCNT-C_3N_4(63), in which a peak at 286.9 eV can be assigned to the presence of sp^3 C-N species (See Figure S2) [47,48]. These observations might indicate that *g*-C_3N_4 has not been formed in MWCNT-C_3N_4(63) composite, but some amorphous CN structure might be present in that sample. This could be a consequence of the high amount of dicyandiamide that remains on the MWCNT in the first step of the composite preparation that impedes the adequate cyclization reactions necessary for C_3N_4 formation.

Concerning the XPS spectra of Pd (Figure 4 (b)), a typical Pd 3d XPS spectrum shows two peaks corresponding to the Pd $3d_{3/2}$ (at higher binding energies) and Pd $3d_{5/2}$

(at lower binding energies) electron transitions, which can be deconvoluted into two different peaks attributed to the presence of Pd species with different electronic properties [49]. The Pd XPS spectrum of Pd/MWCNT and Pd/C_3N_4 display these typical signals, corresponding to the presence of Pd in metallic state and Pd^{2+}. As can be observed, Pd species are mainly as Pd^{2+} in Pd/C_3N_4 compared to Pd/MWCNT, which may be related to the Pd-N interactions. It is well-known that the nitrogen groups present on the support are responsible for the Pd-N interaction, which leads to the stabilization of Pd^{2+} species, even after the utilization of a strong reduction agent during the preparation of the catalysts [50].

As seen in Figure 4 (b), a new Pd species is observed in the Pd XPS spectra of Pd/MWCNT-C_3N_4 catalysts. In this case, three peaks for each electronic transition are distinguished: Pd in the metallic state (~ 335.9 eV), Pd^{2+} (~ 337.4 eV), and a new species with a more deficient electronic density located at higher binding energies (~ 338.7eV). The existence of such deficient electron density Pd species is attributed to the Pd^{2+}-N interaction [35,37]. The shift observed in Pd spectra of Pd/MWCNT-C_3N_4(16)-(38) compared to Pd/C_3N_4 can be related to an improved Pd-N interaction occurring because of the more efficient distribution of C_3N_4 layers on the MWCNT. Probably, a lower number of layer stacking in C_3N_4, due to its distribution on the MWCNT, improves the interaction between the N-containing ligands and the Pd species. Also, the smaller particles present in Pd/MWCNT-C_3N_4(16)-(38) catalysts could be responsible for the shift observed in Pd spectra.

Interestingly, Pd/MWCNT-C_3N_4(63) shows a fourth contribution in the Pd 3d spectrum ($Pd^{\delta-}$). As observed, a new electron-rich Pd species (located at 334.3 eV) is distinguished in that catalyst, indicating that Pd has a different electronic environment. This is in good agreement with the differences appreciated in C 1s and N 1s spectra of

Pd/MWCNT-C_3N_4(63) and it might be due to the existence of C-N species which are different from *g*-C_3N_4 contained in the Pd/MWCNT-C_3N_4 with lower nitrogen contents. These observations are in agreement with the presence of amorphous C_3N_4 in the MWCNT-C_3N_4(63) sample.

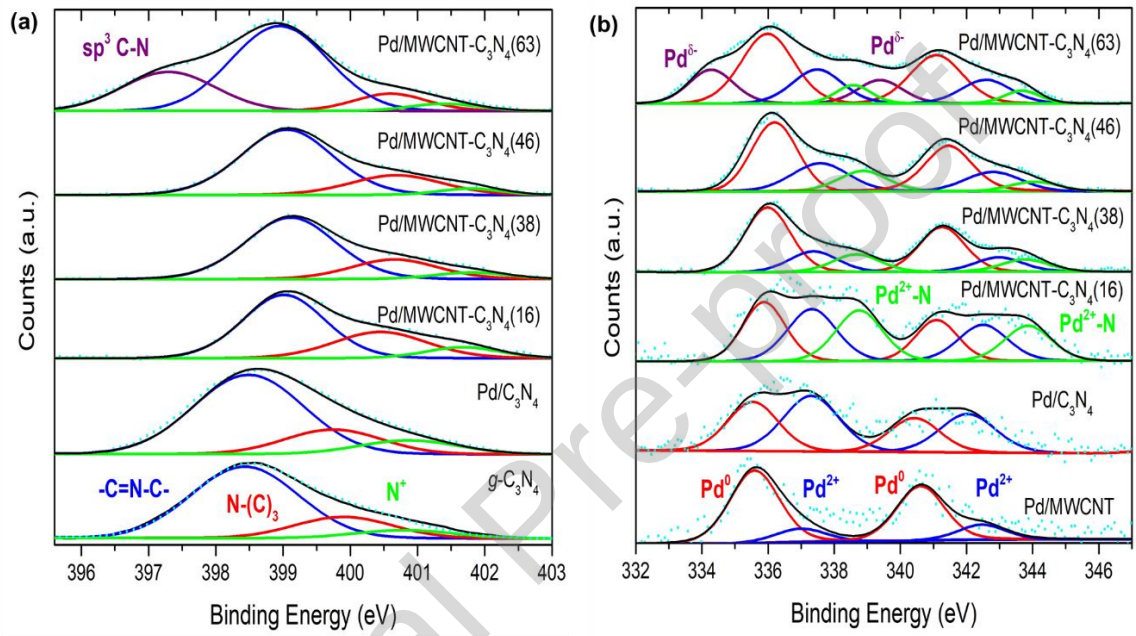

Figure 4. XPS spectra of (a) N 1s and (b) Pd 3d.

The catalysts based on MWCNT-C_3N_4 composite supports with different composition and those supported on pristine MWCNTs and C_3N_4 were evaluated in the dehydrogenation of formic acid at 75 ºC. The gas evolution profiles are plotted in Figure 5 together with the initial TOF values (h^{-1}) expressed as a function of the average NP size determined for each sample. The volume of gas corresponds to the production of H_2 and CO_2 generated from formic acid, according to the following reaction:

$$HCOOH \leftrightarrow H_2 + CO_2$$

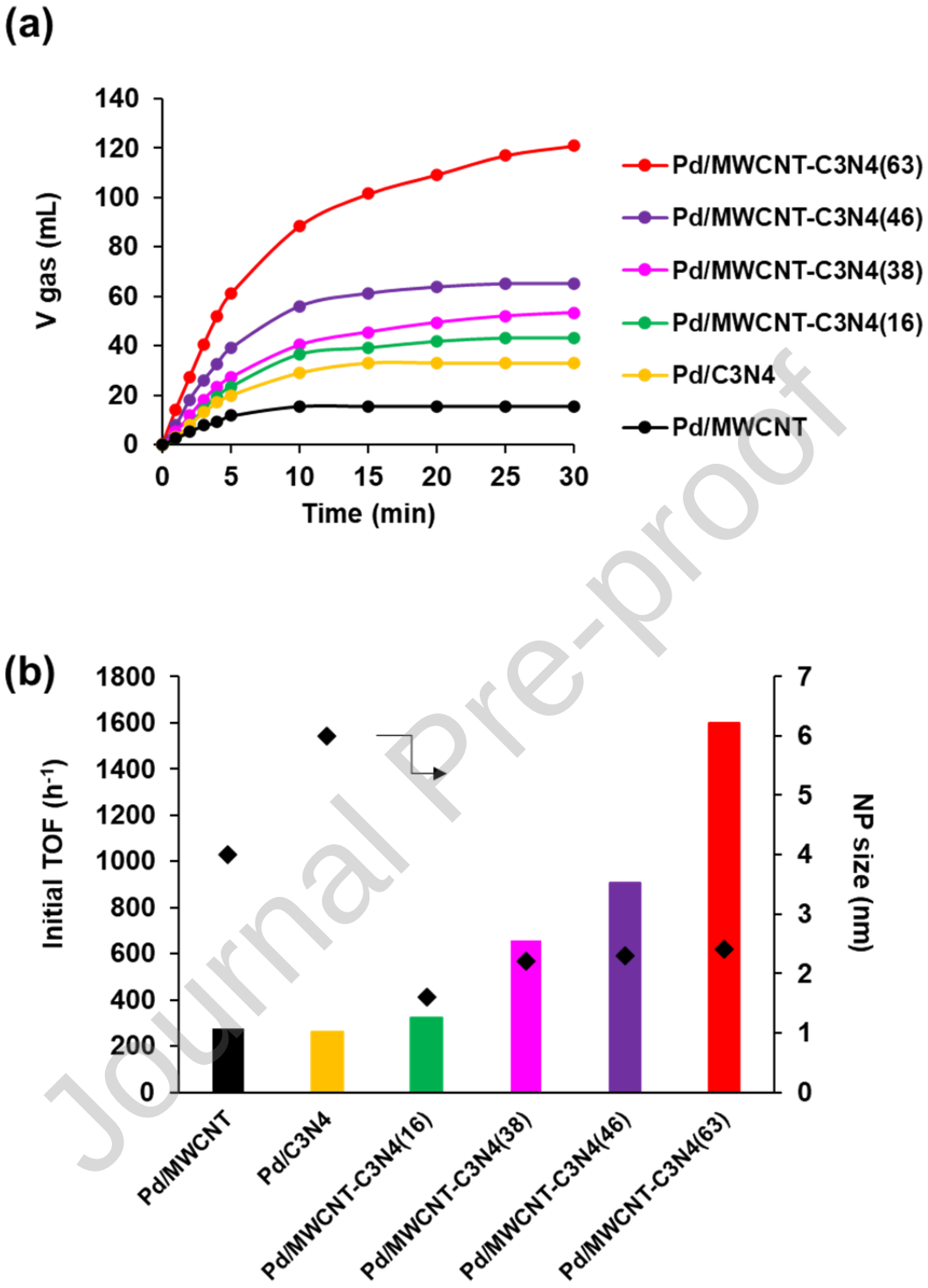

Figure 5. (a) Gas evolution profiles achieved with Pd/MWCNT, Pd/C_3N_4, and the Pd/MWCNT-C_3N_4 catalysts; (b) Initial TOF values (h^{-1}) calculated after 1 min of reaction and based on the total Pd atoms, and referred to the average NP size.

As can be seen in the results plotted in Figure 5, the catalytic activity strongly depended on the composition of the support. The enhancement observed in C_3N_4-containing catalysts can be related to the basicity of the materials and their better dispersibility in the reaction solution as compared to Pd/MWCNT. None of the samples showed induction time and the generation of gas proceed smoothly with time at the beginning of the reaction. Those catalysts based on pure MWCNTs and C_3N_4 (Pd/MWCNT and Pd/C_3N_4, respectively) displayed a poor or moderate activity, generating only 15.6 and 33.0 mL of gas after 30 min of reaction, respectively. However, the catalytic performance enhanced significantly upon using composite supports, and the generated gas increasing with the content of C_3N_4, producing 121 mL of gas after 30 min with Pd/MWCNT-C_3N_4(63). The better performance observed for Pd/MWCNT-C_3N_4 catalysts compared to Pd/MWCNT might be also related to the enrichment of the external surface of the composite supports with Pd (See Table 3).

As for the initial TOF values, the same tendency was observed. Pd/MWCNT and Pd/C_3N_4 had initial TOF values (calculated based on the total Pd content) of 276 and 261 h^{-1}, respectively, but it increased significantly for those catalysts with composite supports, reaching a maximum of 1597 h^{-1} for Pd/MWCNT-C_3N_4(63). These observations indicated that the composition of the MWCNT-C_3N_4 support is a crucial aspect that serves to modulate the catalytic performance. As suggested by the results of Figure 5 (b), in the present catalytic system there is not a clear relationship between the catalytic activity and the average NP size, neither in terms of the total volume of gas generated nor in terms of the initial TOF value, but the smaller NPs observed in the Pd/MWCNT-C_3N_4 catalysts may contribute to the better activity of those samples compared to Pd/MWCNT and Pd/C_3N_4. However, very different results were achieved for catalysts with very similar average NP size (i.e. Pd/MWCNT-C_3N_4(38) and

Pd/MWCNT-C_3N_4(63) had an average NP size of 2.2 and 2.4 nm, respectively, and they generated 53 and 121 mL of gas after 30 min of reaction, with an initial TOF of 656 and 1597 h^{-1}, respectively). That observation suggests that there might be some other important factors, such as the electronic properties of Pd species that also control the catalytic activity of the samples in the dehydrogenation of formic acid. The TOF value achieved by Pd/MWCNT-C_3N_4(63) (1597 h^{-1}), is higher than that attained by other Pd-based catalysts reported in other studies (Au_3Pd_1/C, 407.5 h^{-1} [51]; Pd/$CN_{0.25}$, 752 h^{-1} [52]; Pd/N-HTC (n.r.), 1214 h^{-1} [37]; Pd/NHPC-NH_2, 1265 h^{-1} [53]; Pd/HTNC-950, 1631 h^{-1} [54]; Au_2Pd_8/SBA-15-Amine, 1786 h^{-1} [55]; Pd/MSC-30, 2623 h^{-1} [56]; etc.).

The improved performance achieved by Pd/MWCNT-C_3N_4 compared to Pd/MWCNT and Pd/C_3N_4 might be also related to the electronic properties of Pd species present in the samples. As discussed before, electron-deficient Pd species were detected in those catalysts based on composite supports. Such species have been shown to play an important role in the adsorption of formate ions on the surface of Pd NPs, which takes place in the first reaction step [14]. However, the much superior activity exhibited by Pd/MWCNT-C_3N_4(63) might be also related to the presence of a higher amount of electron-rich Pd species observed in that catalyst, which also contains Pd species with the highest electron density among the tested catalysts. It was postulated that such electron-rich Pd species participate in the second reaction step, which is the cleavage of the C-H bond of the adsorbed formate ion. Such a step is the rate-determining step [14,57]. The proposed reaction mechanism is schematized in Figure 6.

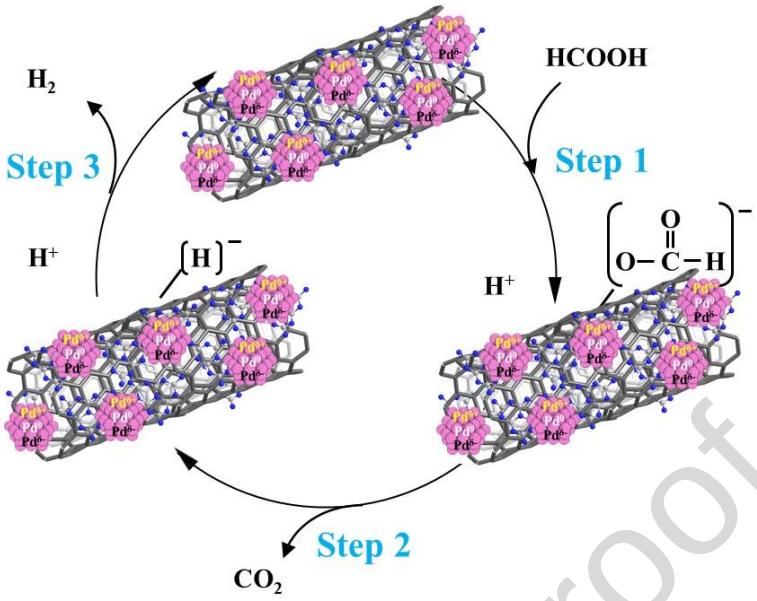

Figure 6. Proposed reaction mechanism.

Interestingly, the catalyst with the best activity (Pd/MWCNT-C_3N_4(63)), has an initial TOF value of 4258 h^{-1} calculated based on the surface Pd atoms, while it was calculated to be of 1227 and 1742 h^{-1} for Pd/MWCNT and Pd/C_3N_4, respectively. That value is higher than many of the Pd-based catalysts reported elsewhere for TOF values calculated considering only the surface atoms (Pd nanoparticles supported on a carbon black (Pd/C), TOF of 853 h^{-1} [58]; Pd nanoparticles encapsulated within carbon nanotubes (Pd-CNTs-in), TOF of 1185 h^{-1} [59]; Pd nanoparticles anchored on amino-functionalized hierarchically porous carbon (Pd/NHPC-NH_2), TOF of 3798 h^{-1} [53]; ultrafine trimetallic CoAuPd NPs with high content of Co immobilized on the pores of metal-organic frameworks MIL-101-NH_2 ($Co_{48}Au_5Pd_{47}$@MIL-101-NH_2), TOF of 361 h^{-1} [60]; etc.).

4. Conclusions

A series of Pd-based catalysts have been prepared on composite supports formed by MWCNTs and *g*-C_3N_4 with various composition. The resulting Pd/MWCNT-C_3N_4 catalysts had a much smaller average NPs size than those supported on pure MWCNT and *g*-C_3N_4, which is attributed to the formation of C_3N_4 domains on the surface of MWCNT, thus serving as efficient anchoring sites for the metal NPs. It was observed that the composition of the MWCNT-C_3N_4 supports is also important to modulate the electronic properties of the supported Pd nanoparticles, thus creating Pd species with different environments.

Pd/MWCNT-C_3N_4 catalysts were evaluated in the dehydrogenation of formic acid, showing improved performance compared to Pd/MWCNT and Pd/C_3N_4. It was observed that the final volume of gas generated increased with the C_3N_4 content. The enhanced catalytic performance achieved by Pd/MWCNT-C_3N_4 catalysts can be related to several factors, such as the control of the NP size, the modification of the electronic properties of the Pd species, the basicity of the materials and the better dispersibility of Pd/MWCNT-C_3N_4 catalysts in the reaction solution as compared to Pd/MWCNT. Among investigated, Pd/MWCNT-C_3N_4(63) was the most promising, with an initial TOF value of 1597 h^{-1}, considering the total Pd content, and 4258 h^{-1} considering the surface Pd atoms.

ACKNOWLEDGMENT

The present work was financed by the MICINN, FEDER (RTI2018-095291-B-I00). MNG thanks the Plan GenT project from GV (CDEIGENT / 2018/027) for the financial support. DST thanks MICINN for the “Juan de la Cierva” contract (IJCI-2016-27636),

and the Vicerrectorado de Investigación y Transferencia de Conocimiento de la Universidad de Alicante (GRE19-16).

Reference

[1] K. Mazloomi, C. Gomes, Hydrogen as an energy carrier: Prospects and challenges, Renew. Sustain. Energy Rev. 16 (2012) 3024–3033. doi:10.1016/j.rser.2012.02.028.

[2] D. Salinas-Torres, M. Navlani-García, K. Mori, Y. Kuwahara, H. Yamashita, Nitrogen-doped carbon materials as a promising platform toward the efficient catalysis for hydrogen generation, Appl. Catal. A Gen. 571 (2019) 25–41. doi:10.1016/J.APCATA.2018.11.034.

[3] G. Sievi, D. Geburtig, T. Skeledzic, A. Bösmann, P. Preuster, O. Brummel, F. Waidhas, M.A. Montero, P. Khanipour, I. Katsounaros, J. Libuda, K.J.J. Mayrhofer, P. Wasserscheid, Towards an efficient liquid organic hydrogen carrier fuel cell concept, Energy Environ. Sci. 12 (2019) 2305–2314. doi:10.1039/C9EE01324E.

[4] P. Preuster, C. Papp, P. Wasserscheid, Liquid Organic Hydrogen Carriers (LOHCs): Toward a Hydrogen-free Hydrogen Economy, Acc. Chem. Res. 50 (2017) 74–85. doi:10.1021/acs.accounts.6b00474.

[5] D. Geburtig, P. Preuster, A. Bösmann, K. Müller, P. Wasserscheid, Chemical utilization of hydrogen from fluctuating energy sources – Catalytic transfer hydrogenation from charged Liquid Organic Hydrogen Carrier systems, Int. J. Hydrogen Energy. 41 (2016) 1010–1017. doi:10.1016/j.ijhydene.2015.10.013.

[6] P.C. Rao, M. Yoon, Potential Liquid-Organic Hydrogen Carrier (LOHC) Systems: A Review on Recent Progress, Energies . 13 (2020) 6040.

doi:10.3390/en13226040.

[7] P.M. Modisha, C.N.M. Ouma, R. Garidzirai, P. Wasserscheid, D. Bessarabov, The Prospect of Hydrogen Storage Using Liquid Organic Hydrogen Carriers, Energy and Fuels. 33 (2019) 2778–2796. doi:10.1021/acs.energyfuels.9b00296.

[8] D. Koutsonikolas, S. Kaldis, V.T. Zaspalis, G.P. Sakellaropoulos, Potential application of a microporous silica membrane reactor for cyclohexane dehydrogenation, Int. J. Hydrogen Energy. 37 (2012) 16302–16307. doi:10.1016/j.ijhydene.2012.02.076.

[9] K. Oda, K. Akamatsu, T. Sugawara, R. Kikuchi, A. Segawa, S. Nakao, Dehydrogenation of Methylcyclohexane To Produce High-Purity Hydrogen Using Membrane Reactors with Amorphous Silica Membranes, Ind. Eng. Chem. Res. 49 (2010) 11287–11293. doi:10.1021/ie101210x.

[10] N. Jiang, K.S.R. Rao, M.-J. Jin, S.-E. Park, Effect of hydrogen spillover in decalin dehydrogenation over supported Pt catalysts, Appl. Catal. A Gen. 425–426 (2012) 62–67. doi:10.1016/j.apcata.2012.03.001.

[11] P.T. Aakko-Saksa, C. Cook, J. Kiviaho, T. Repo, Liquid organic hydrogen carriers for transportation and storing of renewable energy – Review and discussion, J. Power Sources. 396 (2018) 803–823. doi:10.1016/J.JPOWSOUR.2018.04.011.

[12] M. Taube, D.W.T. Rippin, D.L. Cresswell, W. Knecht, A system of hydrogen-powered vehicles with liquid organic hydrides, Int. J. Hydrogen Energy. 8 (1983) 213–225. doi:10.1016/0360-3199(83)90067-8.

[13] M. Martis, K. Mori, K. Fujiwara, W.-S. Ahn, H. Yamashita, Amine-

functionalized MIL-125 with imbedded palladium nanoparticles as an efficient catalyst for dehydrogenation of formic acid at ambient temperature, J. Phys. Chem. C. 117 (2013). doi:10.1021/jp4069027.

[14] K. Mori, M. Dojo, H. Yamashita, Pd and Pd-Ag nanoparticles within a macroreticular basic resin: An efficient catalyst for hydrogen production from formic acid decomposition, ACS Catal. 3 (2013) 1114–1119. doi:10.1021/cs400148n.

[15] R. van Putten, T. Wissink, T. Swinkels, E.A. Pidko, Fuelling the hydrogen economy: Scale-up of an integrated formic acid-to-power system, Int. J. Hydrogen Energy. 44 (2019) 28533–28541. doi:10.1016/J.IJHYDENE.2019.01.153.

[16] M. Navlani-García, K. Mori, A. Nozaki, Y. Kuwahara, H. Yamashita, Screening of Carbon-Supported PdAg Nanoparticles in the Hydrogen Production from Formic Acid, Ind. Eng. Chem. Res. 55 (2016) 7612–7620. doi:10.1021/acs.iecr.6b01635.

[17] M. Navlani-García, M. Martis, D. Lozano-Castelló, D. Cazorla-Amorós, K. Mori, H. Yamashita, Investigation of Pd nanoparticles supported on zeolites for hydrogen production from formic acid dehydrogenation, Catal. Sci. Technol. 5 (2015) 364–371. doi:10.1039/c4cy00667d.

[18] D.A. Bulushev, L.G. Bulusheva, S. Beloshapkin, T. O'Connor, A. V. Okotrub, K.M. Ryan, Pd clusters supported on amorphous, low-porosity carbon spheres for hydrogen production from formic acid, ACS Appl. Mater. Interfaces. 7 (2015) 8719–8726. doi:10.1021/acsami.5b00983.

[19] O.Y. Podyacheva, D.A. Bulushev, A.N. Suboch, D.A. Svintsitskiy, A.S. Lisitsyn,

E. Modin, A. Chuvilin, E.Y. Gerasimov, V.I. Sobolev, V.N. Parmon, Highly Stable Single-Atom Catalyst with Ionic Pd Active Sites Supported on N-Doped Carbon Nanotubes for Formic Acid Decomposition, ChemSusChem. 11 (2018) 3724–3727. doi:10.1002/cssc.201801679.

[20] J. García-Aguilar, M. Navlani-García, Á. Berenguer-Murcia, K. Mori, Y. Kuwahara, H. Yamashita, D. Cazorla-Amorós, Evolution of the PVP-Pd surface interaction in nanoparticles through the case study of formic acid decomposition, Langmuir. 32 (2016) 12110–12118. doi:10.1021/acs.langmuir.6b03149.

[21] M. Wen, K. Mori, Y. Futamura, Y. Kuwahara, M. Navlani-García, T. An, H. Yamashita, PdAg Nanoparticles within Core-Shell Structured Zeolitic Imidazolate Framework as a Dual Catalyst for Formic Acid-based Hydrogen Storage/Production, Sci. Rep. 9 (2019) 15675. doi:10.1038/s41598-019-52133-5.

[22] L. Jia, D.A. Bulushev, J.R.H. Ross, Formic acid decomposition over palladium based catalysts doped by potassium carbonate, 259 (2016) 453–459. doi:10.1016/j.cattod.2015.04.008

[23] M. Zacharska, O.Y. Podyacheva, L.S. Kibis, A.I. Boronin, B. V. Senkovskiy, E.Y. Gerasimov, O.P. Taran, A.B. Ayusheev, V.N. Parmon, J.J. Leahy, D.A. Bulushev, Ruthenium Clusters on Carbon Nanofibers for Formic Acid Decomposition: Effect of Doping the Support with Nitrogen, ChemCatChem. 7 (2015) 2910–2917. doi:10.1002/cctc.201500216.

[24] M. Navlani-García, D. Salinas-Torres, D. Cazorla-Amorós, Hydrogen production from formic acid attained by bimetallic heterogeneous pdag catalytic systems, Energies. 12 (2019) 1–27. doi:10.3390/en12214027.

[25] M. Navlani-García, K. Mori, D. Salinas-Torres, Y. Kuwahara, H. Yamashita,

New Approaches Toward the Hydrogen Production From Formic Acid Dehydrogenation Over Pd-Based Heterogeneous Catalysts, Front. Mater. 6 (2019) 44. doi:10.3389/fmats.2019.00044.

[26] M. Navlani-García, D. Salinas-Torres, K. Mori, Y. Kuwahara, H. Yamashita, Photocatalytic Approaches for Hydrogen Production via Formic Acid Decomposition, Top. Curr. Chem. 377 (2019) 27. doi:10.1007/s41061-019-0253-4.

[27] M. Navlani-García, K. Mori, Y. Kuwahara, H. Yamashita, Recent strategies targeting efficient hydrogen production from chemical hydrogen storage materials over carbon-supported catalysts, NPG Asia Mater. 10 (2018) 1–16. doi:10.1038/s41427-018-0025-6.

[28] A.K. Singh, S. Singh, A. Kumar, Hydrogen energy future with formic acid: A renewable chemical hydrogen storage system, 6 (2015) 12–40. doi:10.1039/c5cy01276g.

[29] X. Wang, Q. Meng, L. Gao, Z. Jin, J. Ge, C. Liu, W. Xing, Recent progress in hydrogen production from formic acid decomposition, Int. J. Hydrogen Energy. 43 (2018) 7055–7071. doi: 10.1016/j.ijhydene.2018.02.146.

[30] H. Zhong, M. Iguchi, M. Chatterjee, Y. Himeda, Q. Xu, H. Kawanami, Formic Acid-Based Liquid Organic Hydrogen Carrier System with Heterogeneous Catalysts, Adv. Sustain. Syst. (2018) 1700161. doi:10.1002/adsu.201700161.

[31] D. Mellmann, P. Sponholz, H. Junge, M. Beller, Formic acid as a hydrogen storage material-development of homogeneous catalysts for selective hydrogen release, Chem. Soc. Rev. 45 (2016) 3954–3988. doi:10.1039/C5CS00618J.

[32] D.A. Bulushev, J.R.H. Ross, Towards Sustainable Production of Formic Acid, ChemSusChem. 11 (2018) 821–836. doi:10.1002/cssc.201702075.

[33] X. Chen, Y. Liu, J. Wu, Sustainable production of formic acid from biomass and carbon dioxide, Mol. Catal. 483 (2020) 110716. doi:10.1016/J.MCAT.2019.110716.

[34] K. Mori, H. Tanaka, M. Dojo, K. Yoshizawa, H. Yamashita, Synergic Catalysis of PdCu Alloy Nanoparticles within a Macroreticular Basic Resin for Hydrogen Production from Formic Acid, Chem. - A Eur. J. 21 (2015) 12085–12092. doi:10.1002/chem.201501760.

[35] D.A. Bulushev, M. Zacharska, E. V Shlyakhova, A.L. Chuvilin, Y. Guo, S. Beloshapkin, A. V Okotrub, L.G. Bulusheva, Single Isolated Pd^{2+} Cations Supported on N-Doped Carbon as Active Sites for Hydrogen Production from Formic Acid Decomposition, ACS Catal. 6 (2016) 681–691. doi:10.1021/acscatal.5b02381.

[36] M. Navlani-García, D. Salinas-Torres, K. Mori, A.F. Léonard, Y. Kuwahara, N. Job, H. Yamashita, Insights on palladium decorated nitrogen-doped carbon xerogels for the hydrogen production from formic acid, Catal. Today. 324 (2019) 90–96. doi:10.1016/j.cattod.2018.06.013.

[37] J. Chaparro-Garnica, M. Navlani-García, D. Salinas-Torres, E. Morallón, D. Cazorla-Amorós, Highly Stable N-Doped Carbon-Supported Pd-Based Catalysts Prepared from Biomass Waste for H_2 Production from Formic Acid, ACS Sustain. Chem. Eng. 8 (2020) 15030–15043. doi:10.1021/acssuschemeng.0c05906.

[38] Y. Wu, M. Wen, M. Navlani-García, Y. Kuwahara, K. Mori, H. Yamashita,

Palladium nanoparticles supported on titanium doped graphitic carbon nitride for formic acid dehydrogenation, Chem. - An Asian J. 12 (2017) 860–867. doi:10.1002/asia.201700041.

[39] M. Navlani-garcía, P. Verma, Y. Kuwahara, T. Kamegawa, K. Mori, H. Yamashita, Visible-light-enhanced catalytic activity of Ru nanoparticles over carbon modified g-C3N4, J. Photochem. Photobiol. A. 358 (2018) 327–333. doi:10.1016/j.jphotochem.2017.09.007.

[40] M. Thommes, K. Kaneko, A. V. Neimark, J.P. Olivier, F. Rodriguez-Reinoso, J. Rouquerol, K.S.W. Sing, Physisorption of gases, with special reference to the evaluation of surface area and pore size distribution (IUPAC Technical Report), Pure Appl. Chem. (2015). doi:10.1515/pac-2014-1117.

[41] A. Ortega-Murcia, M. Navlani-García, E. Morallón, D. Cazorla-Amorós, MWCNT-Supported PVP-Capped Pd Nanoparticles as Efficient Catalysts for the Dehydrogenation of Formic Acid, Front. Chem. 8 (2020) 359. doi:10.3389/fchem.2020.00359.

[42] M. Faisal, A.A. Ismail, F.A. Harraz, S.A. Al-Sayari, A.M. El-Toni, M.S. Al-Assiri, Synthesis of highly dispersed silver doped *g*-C_3N_4 nanocomposites with enhanced visible-light photocatalytic activity, Mater. Des. 98 (2016) 223–230. doi:10.1016/j.matdes.2016.03.019.

[43] G. Vilé, D. Albani, M. Nachtegaal, Z. Chen, D. Dontsova, M. Antonietti, N. López, J. Pérez-Ramírez, A Stable Single-Site Palladium Catalyst for Hydrogenations, Angew. Chemie Int. Ed. 54 (2015) 11265–11269. doi:10.1002/anie.201505073.

[44] T.S. Miller, A.B. Jorge, T.M. Suter, A. Sella, F. Corà, P.F. McMillan, Carbon

nitrides: synthesis and characterization of a new class of functional materials, Phys. Chem. Chem. Phys. 19 (2017) 15613–15638. doi:10.1039/C7CP02711G.

[45] E. Raymundo-Piñero, D. Cazorla-Amorós, A. Linares-Solano, J. Find, U. Wild, R. Schlögl, Structural characterization of N-containing activated carbon fibers prepared from a low softening point petroleum pitch and a melamine resin, Carbon. 40 (2002) 597–608. doi:10.1016/S0008-6223(01)00155-5.

[46] J.T. Titantah, D. Lamoen, Carbon and nitrogen 1s energy levels in amorphous carbon nitride systems: XPS interpretation using first-principles, Diam. Relat. Mater. 16 (2007) 581–588. doi:https://doi.org/10.1016/j.diamond.2006.11.048.

[47] X. Lu, T.H. Tan, Y.H. Ng, R. Amal, Highly Selective and Stable Reduction of CO_2 to CO by a Graphitic Carbon Nitride/Carbon Nanotube Composite Electrocatalyst, Chem. – A Eur. J. 22 (2016) 11991–11996. doi:https://doi.org/10.1002/chem.201601674.

[48] Y. Zheng, Y. Jiao, Y. Zhu, L.H. Li, Y. Han, Y. Chen, A. Du, M. Jaroniec, S.Z. Qiao, Hydrogen evolution by a metal-free electrocatalyst, Nat. Commun. 5 (2014) 3783. doi:10.1038/ncomms4783.

[49] M. Navlani-García, I. Miguel-García, Á. Berenguer-Murcia, D. Lozano-Castelló, D. Cazorla-Amorós, H. Yamashita, Pd/zeolite-based catalysts for the preferential CO oxidation reaction: Ion-exchange, Si/Al and structure effect, Catal. Sci. Technol. 6 (2016) 2623–2632. doi:10.1039/c5cy02044a.

[50] F. Jiang, W. Tan, H. Chen, L. Tan, J. Liu, Effective catalytic hydrodechlorination of chlorophenoxyacetic acids over Pd/graphitic carbon nitride, RSC Adv. 5 (2015) 51841–51851. doi:10.1039/C5RA07913F.

[51] X.T. Guo, J. Zhang, J.C. Chi, Z.H. Li, Y.C. Liu, X.R. Liu, S.Y. Zhang, Efficient dehydrogenation of a formic acid-ammonium formate mixture over Au_3Pd_1 catalyst, RSC Adv. 9 (2019) 5995–6002. doi:10.1039/c8ra09534e.

[52] Q.-Y. Bi, J.-D. Lin, Y.-M. Liu, H.-Y. He, F.-Q. Huang, Y. Cao, Dehydrogenation of Formic Acid at Room Temperature: Boosting Palladium Nanoparticle Efficiency by Coupling with Pyridinic-Nitrogen-Doped Carbon, Angew. Chemie - Int. Ed. 55 (2016) 1–6. doi:10.1002/anie.201605961.

[53] Z. Wang, C. Wang, S. Mao, Y. Gong, Y. Chen, Y. Wang, Pd nanoparticles anchored on amino-functionalized hierarchically porous carbon for efficient dehydrogenation of formic acid under ambient conditions, J. Mater. Chem. A. 7 (2019) 25791–25795. doi:10.1039/C9TA10196A.

[54] M. Yao, W. Liang, H. Chen, X. Zhang, Efficient Hydrogen Production from Formic Acid Using Nitrogen-Doped Activated Carbon Supported Pd, Catal. Letters. 150 (2020) 2377–2384. doi:10.1007/s10562-020-03141-y.

[55] L. Xu, F. Yao, J. Luo, C. Wan, M. Ye, P. Cui, Y. An, Facile synthesis of amine-functionalized SBA-15-supported bimetallic Au-Pd nanoparticles as an efficient catalyst for hydrogen generation from formic acid, RSC Adv. 7 (2017) 4746–4752. doi:10.1039/C6RA26793A.

[56] Q.-L. Zhu, N. Tsumori, Q. Xu, Sodium hydroxide-assisted growth of uniform Pd nanoparticles on nanoporous carbon MSC-30 for efficient and complete dehydrogenation of formic acid under ambient conditions, Chem. Sci. 5 (2014) 195-199. doi:10.1039/C3SC52448E.

[57] Q. Lv, Q. Meng, W. Liu, N. Sun, K. Jiang, L. Ma, Z. Peng, W. Cai, C. Liu, J. Ge, L. Liu, W. Xing, Pd–PdO Interface as Active Site for HCOOH Selective

Dehydrogenation at Ambient Condition, J. Phys. Chem. C. 122 (2018) 2081–2088. doi:10.1021/acs.jpcc.7b08105.

[58] J. Li, W. Chen, H. Zhao, X. Zheng, L. Wu, H. Pan, J. Zhu, Y. Chen, J. Lu, Size-dependent catalytic activity over carbon-supported palladium nanoparticles in dehydrogenation of formic acid, J. Catal. 352 (2017) 371–381. doi:10.1016/j.jcat.2017.06.007.

[59] T.Y. Ding, Z.G. Zhao, M.F. Ran, Y.Y. Yang, Superior activity of Pd nanoparticles confined in carbon nanotubes for hydrogen production from formic acid decomposition at ambient temperature, J. Colloid Interface Sci. (2019) 474-480. doi:10.1016/j.jcis.2018.12.017.

[60] P. Zhao, W. Xu, D. Yang, W. Luo, G. Cheng, Metal-Organic Framework Immobilized CoAuPd Nanoparticles with High Content of Non-precious Metal for Highly Efficient Hydrogen Generation from Formic Acid, ChemistrySelect. 1 (2016) 1400–1404. doi:10.1002/slct.201600397.

Graphical abstract

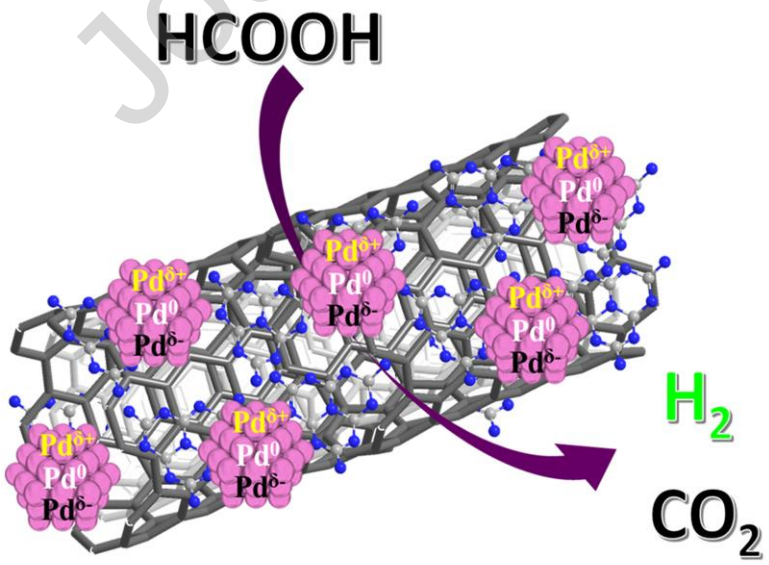

CREDIT AUTHORS STATEMENT

- M. Navlani-García: Conceptualization, Methodology, Investigation, Writing- original draft, review & editing, Funding acquisition.
- D. Salinas-Torres: Conceptualization, Methodology, Writing - review & editing.
- F.D. Vázquez-Álvarez: Methodology and Investigation
- D. Cazorla-Amorós: Conceptualization, Project administration, Supervision, Writing - review & editing, Funding acquisition.

Declaration of interests

☒ The authors declare that they have no known competing financial interests or personal relationships that could have appeared to influence the work reported in this paper.

☐The authors declare the following financial interests/personal relationships which may be considered as potential competing interests:

Highlights

- Pd nanoparticles supported on MWCNT-C_3N_4 were evaluated in the FA dehydrogenation
- The composition of the support controls the properties of the Pd NPs
- High electron density Pd species are formed in Pd/MWCNT-C_3N_4 catalysts
- The catalyst with 63 wt.% of C_3N_4 had the best activity (TOF value of 4258 h^{-1})